SANDIA REPORT

SAND82—0345 • UC—60
Unlimited Release
Printed October 1982

Finite Element Analysis and Modal Testing of a Rotating Wind Turbine

Thomas G. Carne, Donald W. Lobitz,
Arlo R. Nord, Robert A. Watson

Prepared by
Sandia National Laboratories
Albuquerque, New Mexico 87185 and Livermore, California 94550
for the United States Department of Energy
under Contract DE-AC04-76DP00789

Issued by Sandia National Laboratories, operated for the United States Department of Energy by Sandia Corporation.

Available to DOE and DOE contractors from
Office of Scientific and Technical Information
PO Box 62
Oak Ridge, TN 37831

Prices available from (615) 576-8401, FTS 626-8401

Available to the public from
National Technical Information Service
US Department of Commerce
5285 Port Royal Rd
Springfield, VA 22161

NTIS price codes
Printed copy: A02
Microfiche copy: A01

SAND82-0345

FINITE ELEMENT ANALYSIS AND MODAL TESTING OF A ROTATING WIND TURBINE*

T. G. Carne
D. W. Lobitz
A. R. Nord
R. A. Watson
Sandia National Laboratories
Albuquerque, NM

Abstract

A finite element procedure, which includes geometric stiffening, and centrifugal and Coriolis terms resulting from the use of a rotating coordinate system, has been developed to compute the mode shapes and frequencies of rotating structures. Special application of this capability has been made to Darrieus, vertical axis wind turbines. In a parallel development effort, a technique for the modal testing of a rotating vertical axis wind turbine has been established to measure modal parameters directly. Results from the predictive and experimental techniques for the modal frequencies and mode shapes are compared over a wide range of rotational speeds.

---

* This work was performed at Sandia National Laboratories and was supported by the U. S. Department of Energy under contract number DE-AC04-76DP00789.

Table of Contents

Introduction

Over the past several years, wind energy has been considered as a potentially viable option in the search for renewable energy sources. The feasibility of tapping this source depends on the ability to design extraction devices which are both safe and reliable, and, can be produced at low cost. The extraction device of interest here is the vertical axis wind turbine (VAWT) shown in Figure 1. As dynamic effects can be substantial due to the periodic nature of the aerodynamic loading, the design process must depend on accurate predictive tools and/or measurement techniques for determining the dynamic response characteristics of the turbine.

Determination of modal characteristics is of paramount importance in that, with this information, resonant behavior can be avoided. In rotating structures, the acquisition of these characteristics is complicated by their dependence on the structure's rotational speed. Therefore, special methods have to be employed for both the predictive and experimental procedures.

In this paper predictive as well as experimental techniques are described for identifying the modal characteristics of a VAWT. Results from each method are obtained and compared for a two-meter turbine.

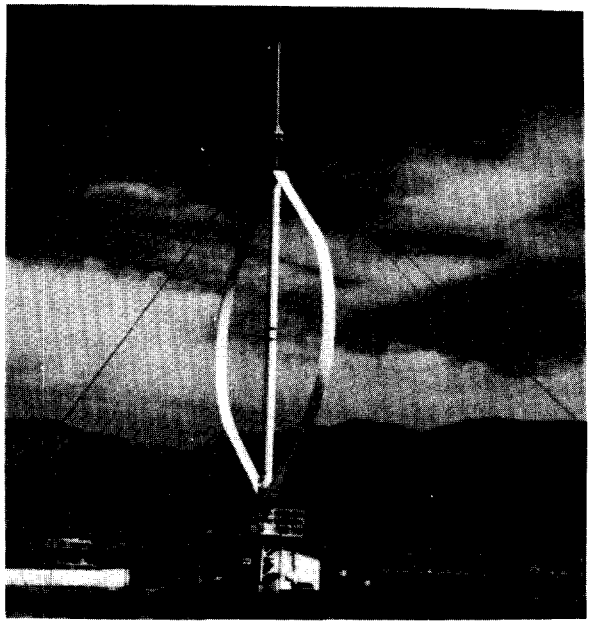

Fig. 1 The Sandia 17-m Research Turbine

The predictive technique developed here is based on the finite element method in order to take advantage of its superior versatility. As the turbine is modeled in a frame which rotates at the turbine operating speed (assumed constant), rotating coordinate system effects must be taken into account. Within this frame, the motions of the turbine are assumed to be small.

The finite element method has been used previously to predict the modal characteristics of rotating structures. Several investigators,[1-4] have applied the method to structures which are comprised of rotating beams reminiscent of fan or helicopter blades. However, in these cases some of the rotating coordinate system effects are neglected. This may be justified since, for these types of structures, motions normal to the axis of rotation are relatively small. For the vertical axis wind turbine, this is not the case and these effects cannot be omitted. A method described in Ref. 5 uses finite elements to obtain the eigenvalue solution to the spinning skylab problem. This method, which is similar to the one used here for the analysis of the VAWT, includes all rotating coordinate system effects.

Other techniques which have been used to obtain dynamic characteristics of rotating structures include various Galerkin procedures, the modal method, and the component mode method in combination with various eigensolution schemes. In Ref. 6, the Garlerkin method is used in conjunction with an asymptotic expansion technique (the method of multiple time scales) to examine resonance in a spinning, nutating plate. A Galerkin procedure was also used in Ref. 7 where the dynamic response of a horizontal axis wind turbine was studied with Floquet Theory. Refs. 8-10 employ the component mode method in combination with relatively standard eigenvalue extraction procedures to investigate the dynamic characteristics of a VAWT.

A major experimental obstacle in obtaining the natural frequencies and mode shapes of a rotating structure is that mechanisms for exciting the structure while it is rotating must be devised. Also slip-rings or telemetry must be employed for data transmission from the structure. These complications may account for

the minimal amount of reporting for this type of modal testing in the open literature. One reference,[11] however, was found where modal test data were cited for a model propeller blade as a function of rpm. The original work, Ref. 12, may be difficult to acquire.

The remainder of this paper is divided into five sections. The first describes the details of the finite element method used for predicting the modes and frquencies of the rotating turbine. In the second, details of the finite element model are presented. The experimental procedure for the rotating modal test is described in the third. The fourth provides comparisons of the predicted and experimental data. The final section contains the conclusions.

Finite Element Theory for the VAWT

The effects which must be included for an accurate representation of the dynamics of a VAWT relative to a coordinate system rotating at a constant speed, include tension stiffening, and centrifugal and Coriolis terms. Manifestations of the latter primarily appear in the inertia terms of the equations of motion. However, in the finite element context, they result in additions to the damping and stiffness matrices, and the force vector. Specifically, the Coriolis terms produce a skew-symmetric contribution to the damping matrix, and the centrifugal forces result in a steady force plus a negative contribution to the stiffness matrix, referred to here as centrifugal softening. The resulting finite element equations are represented by

$$M\ddot{u} + C\dot{u} - Su + Ku = F_c + F_g, \qquad (1)$$

where M is the classical mass matrix, C is the Coriolis matrix, S is the centrifugal softening matrix, K is the usual stiffness matrix, F_c is a static load vector representing the steady centrifugal force, and F_g represents the gravitational forces which are also steady due to the orientation of the axis of rotation of the turbine. To obtain the modes and frequencies of the turbine as observed in the rotating system, equation (1) is reduced to the following form:

$$M\ddot{u} + C\dot{u} + (K + K_G - S)\, u = 0, \qquad (2)$$

where K_G is the geometric stiffness matrix resulting from the steady centrifugal and gravitational loads. Thus the solutions correspond to small motions about a prestressed state.

Aeroelastic effects have not been included in this analysis. These effects have, however, been incorporated in stability investigations of the VAWT[13] and, while strongly influencing stability, seem to have little effect on the natural frequencies and modes of the turbine. This, coupled with the general experimental observation that VAWTs are relatively stable machines, tends to justify this omission.

The coordinate system employed in this analysis rotates at the turbine operating speed with the origin fixed in space at the base of the tower. As shown in Figure 2, the angular velocity vector is directed vertically along the z axis.

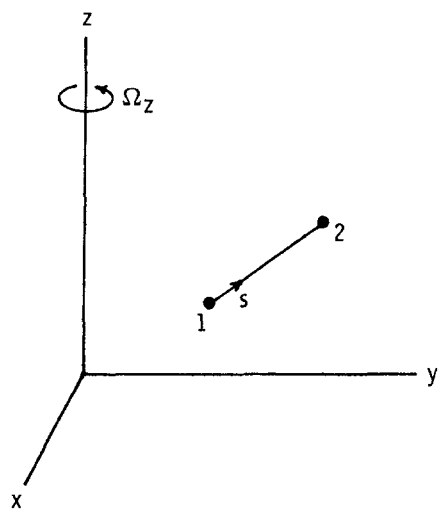

Fig. 2 A Beam Element in the Rotating Frame

The finite element matrices are developed on the basis of the motions that remain small within this rotating frame. The matrices, M, K, and K_G are presented in a number of currently available finite element texts and will not be derived here. On the other hand, the matrices, C and S, which are due to rotating coordinate system effects, are not commonly encountered, and therefore will be developed.

Due to the structural nature of VAWTs, the finite element equations need only be developed for beam elements and concentrated masses. In

order to develop inertia matrices for the beam elements, the displacements, velocities and accelerations are assumed to vary linearly along the length of the element. The mass of the element is concentrated along its axis so that the rotational kinetic energy of the element about its axis is neglected. Using the following equation for the total acceleration at a point in the rotating system,

$$\underset{\sim}{a}_t = \ddot{\underset{\sim}{\mu}} + 2\underset{\sim}{\Omega} \times \dot{\underset{\sim}{\mu}} + \underset{\sim}{\Omega} \times [\underset{\sim}{\Omega} \times (\underset{\sim}{r} + \underset{\sim}{\mu})] \ , \tag{3}$$

where

$\underset{\sim}{a}_t$ is the total acceleration vector, excluding gravitational acceleration,

$\underset{\sim}{r}$, $\underset{\sim}{\mu}$, $\dot{\underset{\sim}{\mu}}$ and $\ddot{\underset{\sim}{\mu}}$ are the original position, the displacement, velocity, and acceleration vectors, respectively, as observed in the rotating coordinate system, and

$\underset{\sim}{\Omega}$ is the fixed angular velocity vector of that system,

an expression for the inertia force due to the elemental mass at that point can be developed. Adopting the linear form for the motion, the initial position, displacement, velocity, and acceleration relative to the rotating frame can be cast in terms of the nodal point values as follows (see Figure 2):

$$\underset{\sim}{r} = P\,\bar{r}, \qquad \underset{\sim}{u} = P\,\bar{u}\ , \qquad \dot{\underset{\sim}{u}} = P\,\dot{\bar{u}}, \qquad \ddot{\underset{\sim}{u}} = P\,\ddot{\bar{u}}\ , \tag{4}$$

where

$$P = \begin{bmatrix} 1-s/\ell & 0 & 0 & s/\ell & 0 & 0 \\ 0 & 1-s/\ell & 0 & 0 & s/\ell & 0 \\ 0 & 0 & 1-s/\ell & 0 & 0 & s/\ell \end{bmatrix},$$

$$\bar{u}^T = \begin{bmatrix} u_{x_1} & u_{y_1} & u_{z_1} & u_{x_2} & u_{y_2} & u_{z_2} \end{bmatrix}, \text{ etc.},$$

s is the arc length variable, and

ℓ is the length of the element.

Note that the overbars denote nodal point values. Specializing $\underset{\sim}{\Omega}$ to $\underset{\sim}{\Omega}^T = [0\ 0\ \Omega_z]$, the second and third terms of equation (3) become

$$2\underset{\sim}{\Omega} \times \dot{\underset{\sim}{\mu}} = 2\Omega_z Q\dot{\bar{u}}\ , \tag{5}$$

$$\underset{\sim}{\Omega} \times [\underset{\sim}{\Omega} \times (\underset{\sim}{r} + \underset{\sim}{\mu})] = -\Omega_z^2\, R(\bar{r} + \bar{u})\ , \tag{6}$$

where

$$Q = \begin{bmatrix} 0 & -1+s/\ell & 0 & 0 & -s/\ell & 0 \\ 1-s/\ell & 0 & 0 & s/\ell & 0 & 0 \\ 0 & 0 & 0 & 0 & 0 & 0 \end{bmatrix},$$

$$R = \begin{bmatrix} 1-s/\ell & 0 & 0 & s/\ell & 0 & 0 \\ 0 & 1-s/\ell & 0 & 0 & s/\ell & 0 \\ 0 & 0 & 0 & 0 & 0 & 0 \end{bmatrix}.$$

Using d'Alembert forces along with the concept of virtual work, the required matrices are obtained as follows:

$$\int_0^\ell \delta u^T \rho \underset{\sim}{a}_t ds = \delta\bar{u}^T \Big[\rho\Big(\int_0^\ell P^T P ds\Big)\ddot{\bar{u}} + 2\rho\Omega_z\Big(\int_0^\ell P^T Q ds\Big)\dot{\bar{u}} - \rho\Omega_z^2\Big(\int_0^\ell P^T R ds\Big)\bar{u} - \rho\Omega_z^2\Big(\int_0^\ell P^T R ds\Big)\bar{r}\Big] \tag{7}$$

where δu^T is the variation in the nodal displacements and ρ is the mass per unit length. The first integral on the right hand side of equation (7) corresponds to the mass matrix; the second, the Coriolis matrix; the third, the centrifugal softening matrix; and the fourth, the centrifgal forces. Of special interest here are the second and third terms which are presented in detail below:

Coriolis

$$2\rho\ell\Omega_z \begin{bmatrix} 0 & -1/3 & 0 & 0 & -1/6 & 0 \\ 1/3 & 0 & 0 & 1/6 & 0 & 0 \\ 0 & 0 & 0 & 0 & 0 & 0 \\ 0 & -1/6 & 0 & 0 & -1/3 & 0 \\ 1/6 & 0 & 0 & 1/3 & 0 & 0 \\ 0 & 0 & 0 & 0 & 0 & 0 \end{bmatrix} \begin{Bmatrix} \dot{u}_{x_1} \\ \dot{u}_{y_1} \\ \dot{u}_{z_1} \\ \dot{u}_{x_2} \\ \dot{u}_{y_2} \\ \dot{u}_{z_2} \end{Bmatrix} \tag{8}$$

Centrifugal Softening

$$\rho\ell\Omega_z^2 \begin{bmatrix} 1/3 & 0 & 0 & 1/6 & 0 & 0 \\ & 1/3 & 0 & 0 & 1/6 & 0 \\ & & 0 & 0 & 0 & 0 \\ & & & 1/3 & 0 & 0 \\ & \text{sym} & & & 1/3 & 0 \\ & & & & & 0 \end{bmatrix} \begin{Bmatrix} u_{x_1} \\ u_{y_1} \\ u_{z_1} \\ u_{x_2} \\ u_{y_2} \\ u_{z_2} \end{Bmatrix} \tag{9}$$

Concentrated masses, such as blade joints, flanges and support bearings, are handled in an entirely similar manner, resulting in the following expressions:

$$\underline{\text{Coriolis}} \qquad\qquad \underline{\text{Centrifugal Softening}}$$

$$2m\Omega_z \begin{bmatrix} 0 & -1 & 0 \\ 1 & 0 & 0 \\ 0 & 0 & 0 \end{bmatrix} \begin{Bmatrix} \dot{u}_{x_1} \\ \dot{u}_{y_1} \\ \dot{u}_{z_1} \end{Bmatrix}, \qquad m\Omega_z^2 \begin{bmatrix} 1 & 0 & 0 \\ 0 & 1 & 0 \\ 0 & 0 & 0 \end{bmatrix} \begin{Bmatrix} u_{x_1} \\ u_{y_1} \\ u_{z_1} \end{Bmatrix}. \tag{10}$$

These concentrated masses possess no rotational kinetic energy. They must, however, be attached to a point which is on the rotating structure.

The matrices, C and S, of equations (1) and (2) are obtained by assembling the contributions from all the beam elements and concentrated masses of the finite element model.

A critical factor in the development of this method is that vector transformations are not required between stationary (groundbased) and rotating coordinate systems. For most VAWTs, the physical connections of the rotor to the ground occur through the tiedown cables and the tower base connection. The stiffness of both of these connection mechanisms is usually isotropic (independent of azimuthal position) and therefore can be represented by massless linear springs which rotate with the turbine and act to restore it to its original position. The associated mass can usually be adequately modeled by concentrated masses placed at appropriate points in the rotating frame.

The eigensystem represented by equation (2) is Hermetian due to the skew-symmetry of the Coriolis matrix. Consequently, it can be shown[14] that the eigenvectors are, in general, complex; but the eigenvalues, which are the squares of the circular frequencies, are real. Thus, with this system, the natural frequencies are purely real or purely imaginary depending on the sign of the real eigenvalues. If structural damping is included, the system loses its Hermetian character and the eigenvalues as well as the eigenvectors are complex. For the present analyses, structural damping has been excluded due to the lightly damped nature of most VAWTs.

Instead of developing a completely independent package for the eigensolution of equation (2), an existing code was modified. With this approach, duplication of such things as input, output, plotting, solution procedures, etc., is avoided. The MacNeal-Schwendler version of NASTRAN[15] was selected here because the modification required was minimal and could be accomplished via DMAP programming, a feature which allows the NASTRAN user to modify the code without actually dealing with the FORTRAN coding. This version contains complex eigensystem solution procedures and also permits the stiffness, mass, and damping matrices to be modified through an input option. Thus, the special matrices required in equation (2), specifically the Coriolis (C) and softening (S) matrices, can be generated externally and read into NASTRAN as input. As the NASTRAN code handles non-symmetric as well as symmetric matrices, no special problems occur due to the skew-symmetry of the Coriolis matrix. The mass (M) and stiffness (K) matrices are generated internally, complete with the effects of geometric stiffening in the stiffness matrix. Additional details on this NASTRAN procedure are presented in the next section.

This analysis package has undergone limited verification due to the lack of available closed form solutions for rotating structures. However, the exact solution for the compressed, whirling shaft with pinned ends provides at least one test case. If the shaft is not spinning, its natural frequencies and corresponding modal solutions are given by

$$\nu_n = \left(\frac{n\pi}{L}\right)^2 \left(\frac{EI}{\rho A}\right)^{1/2} \left[1 - \frac{P}{EI}\left(\frac{L}{n\pi}\right)^2\right]^{1/2}, \tag{11}$$

$$\begin{Bmatrix} u \\ v \end{Bmatrix}_1 = \sin\frac{n\pi}{L} z \begin{Bmatrix} \cos \nu_n t \\ 0 \end{Bmatrix}, \qquad \begin{Bmatrix} u \\ v \end{Bmatrix}_2 = \sin\frac{n\pi}{L} z \begin{Bmatrix} 0 \\ \cos \nu_n t \end{Bmatrix}, \tag{12}$$

where

P is the axial load,

u, v are the transverse displacements, and

E, I, ρ, A, L are the usual physical properties of the shaft.

On the other hand, when the shaft is spinning its natural frequencies, ω_n, relative to the rotating frame are

$$\omega_n = |\nu_n \pm \Omega| \ , \qquad (13)$$

where ν_n is given by equation (11) and Ω is the angular velocity of the shaft. Thus, the non-spinning natural frequencies split into two frequencies, one increasing with angular velocity at a rate of 1 Hz/Hz, and the other decreasing at 1 Hz/Hz. Moreover, the modal solutions become

$$\begin{Bmatrix} u \\ v \end{Bmatrix}_1 = \sin \frac{n\pi}{L} z \begin{Bmatrix} \cos \omega_n t \\ \cos (\omega_n t + \pi/2) \end{Bmatrix},$$
$$\begin{Bmatrix} u \\ v \end{Bmatrix}_2 = \sin \frac{n\pi}{L} z \begin{Bmatrix} \cos \omega_n t \\ \cos (\omega_n t + \frac{3\pi}{2}) \end{Bmatrix}. \qquad (14)$$

Whereas the u and v motions were previously uncoupled in the modes of the non-spinning shaft, now they are coupled, with the motion in one direction ninety degrees out of phase with that in the other. This behavior as well as the natural frequency variation with angular velocity is precisely predicted by the finite element analysis package.

Finite Element Results for the 2-m VAWT

In this section the details of the finite element model used to predict the modes and frequencies of the Sandia 2-m research turbine as a function of rpm are presented. Before doing this, however, a short description of the NASTRAN calculational procedure is in order.

This procedure is based on version 61 of MSC-NASTRAN[15] and utilizes two of the available rigid format options. Using the first of two required data decks, a static analysis with geometric stiffening effects (Rigid Format 64) is performed on the model under the action of centrifugal, gravitational and boundary forces. The resulting modified stiffness matrix is then retained via a modest amount of DMAP programming for use in the subsequent complex eigenvalue analysis (Rigid Format 67) of the second data deck. Along with the necessary structural data, this second deck also includes the "Direct Matrix Input at Grid Points" (DMIG) cards, through which the Coriolis and Centrifugal Softening matrices described in the previous section are input. Because the actual number of DMIG cards required tends to be large, a pre-processing program, FEVD, was written for automation purposes. FEVD reads the NASTRAN structural data deck and extracts information it needs from GRID, CBAR, PBAR, MAT1, CONM2, and RFORCE cards. With this information it constructs the necessary matrices and casts them in terms of DMIG cards. It then inserts these into the second NASTRAN data deck. In this manner, the exercise of including rotating coordinate system effects in NASTRAN is relatively transparent to the user.

NASTRAN provides the user with a choice of two complex eigensolvers. The one which employs the upper Hessenberg method is very efficient but limited to sixty degrees of freedom (the actual number may vary depending on computer installation). The other which utilizes the inverse power method is limited in the number of degrees of freedom only by economic considerations, but requires insight into the location of the desired natural frequencies in the complex plane. For the analysis in this paper, the upper Hessenberg method was used in conjunction with Guyan reduction (also a NASTRAN option) to reduce the number of degrees of freedom from that of the actual model to sixty.

The finite element model of the 2-m VAWT is shown in Figure 3. The actual hardware is displayed in a photograph in Figure 4. The truss tower, which adds a

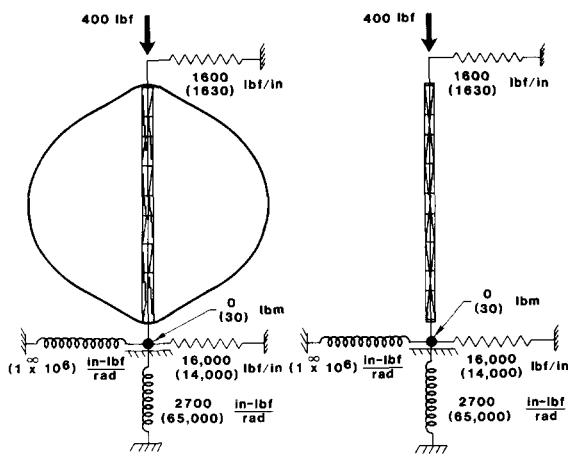

Fig. 3 Finite Element Model of the 2-m VAWT

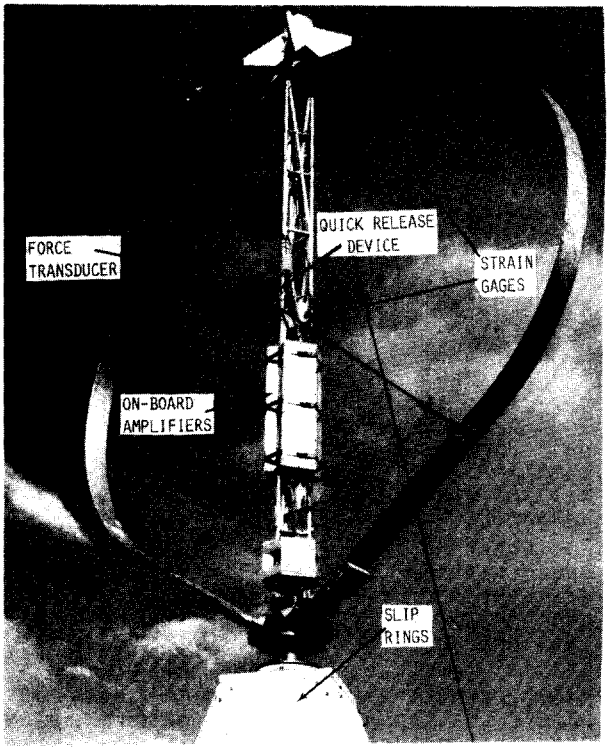

Fig. 4 The Sandia 2-m Turbine with Instrumentation

fair degree of complexity to the model, is represented by 150 beam elements. The blades are modeled with 20 beam elements each. The mass of the hardware associated with the upper bearing and tie-down connections is represented by a concentrated mass placed at the top of the tower. The tie-down cables are modeled with horizontal linear springs and a vertical downward force as shown in Figure 3. The mass of the instrumentation installed on the rotor for the test (which is not negligible compared to the rotor mass) is included through appropriate concentrated masses. The base is modeled as shown in Figure 3, with a concentrated mass in combination with torsional and linear springs. As indicated the springs are equal in the two orthogonal directions, thus producing the desired isotropic effect mentioned in the preceding section.

Using parked test data, the model was moderately tuned by adjusting the parameters associated with the base which, in general, must be estimated. The modified values are given in parentheses in Figure 3. The resulting parked frequencies for the first ten modes are given in Table 1 along with the experimental values. As computed from the table, the average error in the frequencies was reduced from 12 to less than 1 per cent, after tuning. Only the second symmetric flatwise mode deviated by more than 1 per cent, which is most probably caused by inaccurate modeling of the blade-to-tower joint.

Mode identification terminology is given in the second column of Table 1 for the first ten parked modes, and corresponding three-views in Figure 5. In Figure 6, for purposes of comparison, predicted and measured three-views of the 2nd rotor out-of-plane mode are given. This agreement is representative of the first ten modes.

Table 1 Parked Frequency Comparison

Mode Number	Mode Name	Measured Modal Frequency (Hz)	Initial Analytical Frequency (Hz)	Modified Analytical Frequency (Hz)
1	1st Antisymmetric Flatwise	12.3	12.5	12.3
2	1st Symmetric Flatwise	12.5	12.6	12.4
3	1st Rotor Out-of-Plane	15.3	17.1	15.2
4	1st Rotor In-Plane	15.8	17.2	15.9
5	Dumbbell	24.4	22.6	24.4
6	2nd Rotor Out-of-Plane	26.2	30.5	26.2
7	2nd Rotor In-Plane	28.3	30.6	28.0
8	2nd Symmetric Flatwise	29.7	30.9	30.6
9	2nd Antisymmetric Flatwise	31.5	39.7	31.7
10	3rd Rotor Out-of-Plane	36.5	42.3	36.5

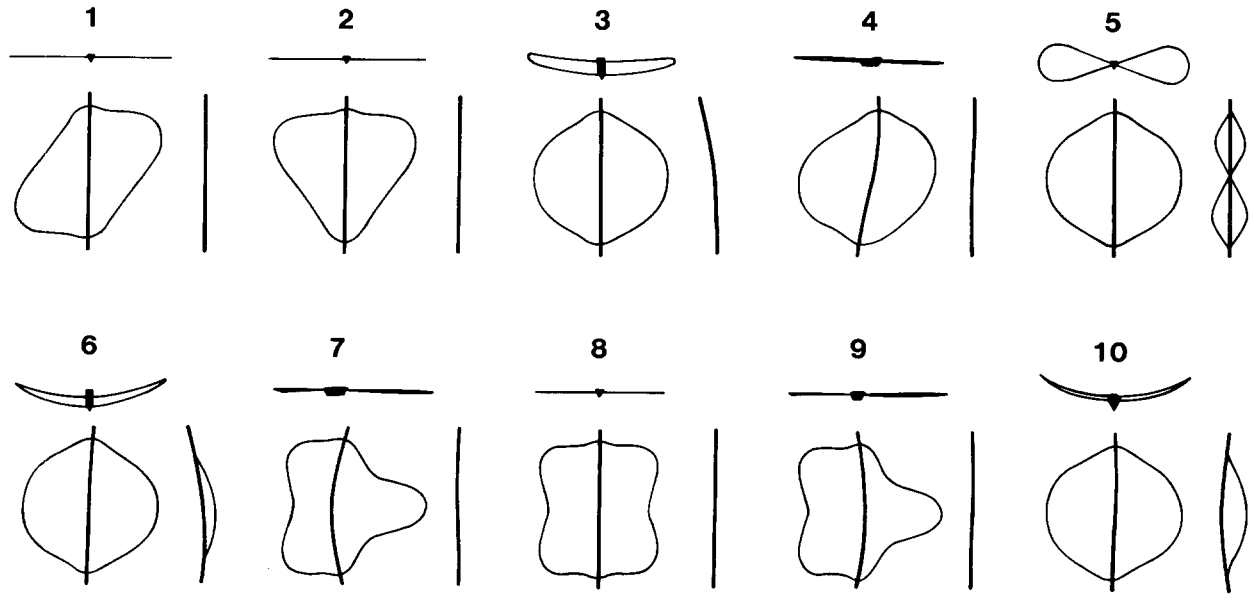

Fig. 5 Predicted Mode Shapes for the Parked 2-m VAWT

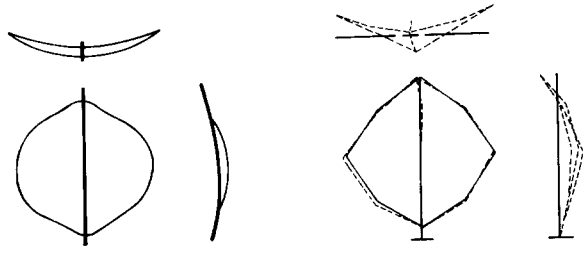

Fig. 6 A Comparison of the Predicted and Measured 2nd Rotor Out-of-Plane Mode of the Parked Turbine

Using the tuned parameters, the fan plot of Figure 7 was produced. The mode numbers on the various curves correspond to the modes identified in Table 1. The variations of the frequencies with rpm are quite complex. While most monotonically increase with rpm, some decrease monotonically. Others increase and then decrease and vice versa. Although more complicated, these variations are similar to those associated with the whirling shaft problem discussed in the previous section.

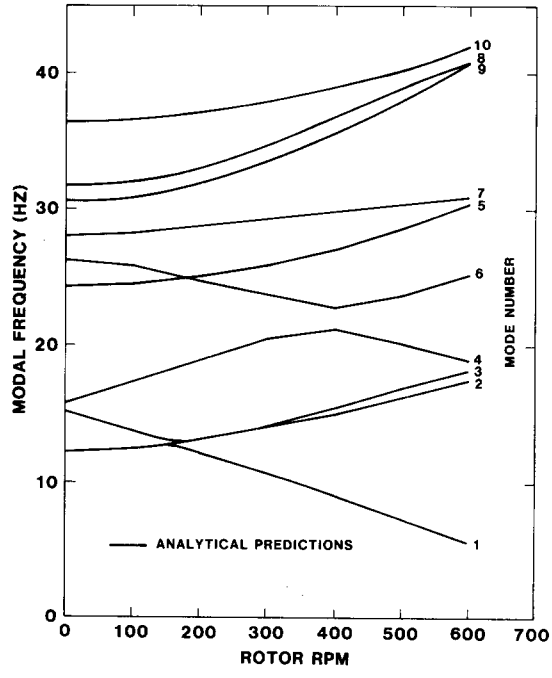

Fig. 7 Predicted Fan Plot for the 2-m VAWT

In addition to complicated frequency variations, the mode shapes also change in character with rpm. Specifically, mode shapes which are completely uncoupled when the turbine is parked become coupled during rotation. In general, the coupling occurs between pairs of parked modes 90° out of phase with each other. In Figure 8 this coupling is shown for the 2nd rotor out-of-plane mode. As the turbine rotates, a mode which is similar to the 1st rotor in-plane mode is drawn into and coupled with the original mode, but at a 90° phase shift. In mathematical terms, the modes change from real to complex when the turbine rotates. Furthermore, as indicated in Figure 8, these complex mode shapes change slightly as a function of rpm.

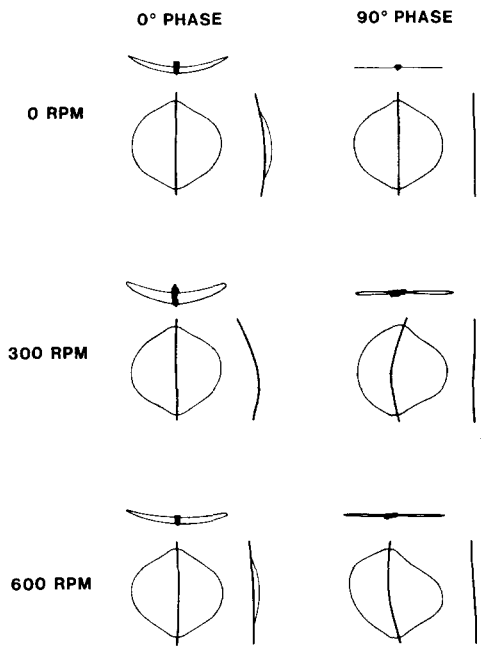

Fig. 8 Predicted Modal Coupling with Turbine Rotation

Experimental Procedure

There are two objectives in developing a modal testing capability for a rotating turbine. First, experimental data on representative hardware is required to verify the accuracy of the finite element analysis technique described above, and secondly, a need exists for an established experimental technique to measure rotating modal frequencies so that, in the absence of other information, design modifications of an existing turbine can be made purely on the basis of the test data.

In this section, the experimental procedures that were developed for modal testing of both the parked and rotating turbine will be described. The general technique of modal testing with a mini-computer based Fast Fourier Transform (FFT) will be discussed briefly, followed by its application to the parked Sandia 2-m research turbine. This particular turbine was selected for the test because of its manageable size and its variable speed capability. Finally, for the rotating modal test, a full description of the instrumentation, the excitation of the structure, and the extraction of the modal parameters from the data will be given.

The FFT technique, which involves exciting the structure with a force having a linear spectrum containing the frequency band of interest, is generally faster and more versatile than the older analog swept-sine technique. The applied force and response are measured in the time domain and transformed to the frequency domain using the FFT. The frequency response function is then computed using the cross-spectral and auto-spectral densities of the applied force and the response. Typically a number of measurements are averaged so as to reduce the effects of uncorrelated noise. A more complete description of FFT modal testing is contained in Ref. 16. The greater versatility of this technique is a result of more relaxed requirements on the excitation. For example, the technique is equally applicable to shaker driven structures or structures excited by an instrumented hammer.

As the first step in the rotating modal test, a detailed parked modal test was conducted. The turbine was extensively instrumented with piezoelectric accelerometers on the blades, tower, and turbine base. Figure 9 shows a diagram of the turbine with the measurement points indicated by numbers. The excitation was provided by an instrumented hammer for impacting either the tower or the blades. The accelerometer and force time histories were filtered, recorded on FM tape, and, using mini-computer based software, digitized and combined to form a set of frequency response functions.

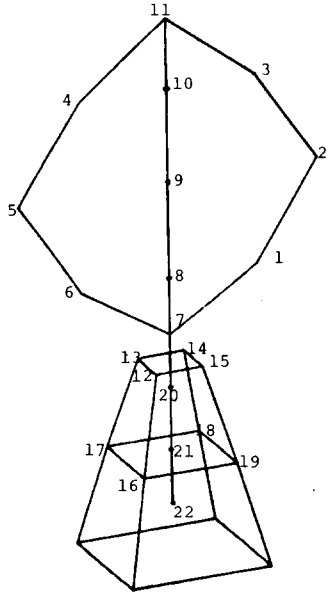

Fig. 9 Measurement Locations for the Parked 2-m VAWT Modal Test

Prior to the test, a two channel analyzer was used to determine the frequency range of interest, the resolution required, and the best locations for the driving points. From this procedure it was determined that all the modes of interest were between ten and sixty Hz. The input force spectrum was tailored for this range, and the time histories were zoomed between its extremes to give a desirable frequency resolution (approximately 0.1 Hz).

Figure 10 shows a typical frequency response function using three samples of data with the magnitude plotted versus frequency. This response function is the response of a blade in the flatwise direction (perpendicular to the blade chord) due to a force input on the tower. The sharp resonant peaks clearly indicate modal frequencies and, because of their sharpness, the corresponding low modal damping. Using additional mini-computer based software[17] with a complete set of frequency response functions (one for each measurement point and direction) as input, the modal frequencies, damping, and mode shapes are computed. Figure 11 shows one view of four of the fourteen modes that were extracted from the data, with the deformed shapes indicated by the dashed lines.

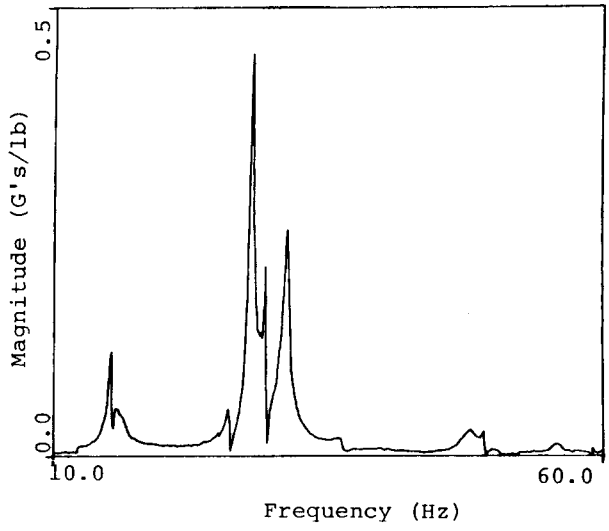

Fig. 10 Typical Frequency Response Function From the Parked Modal Test

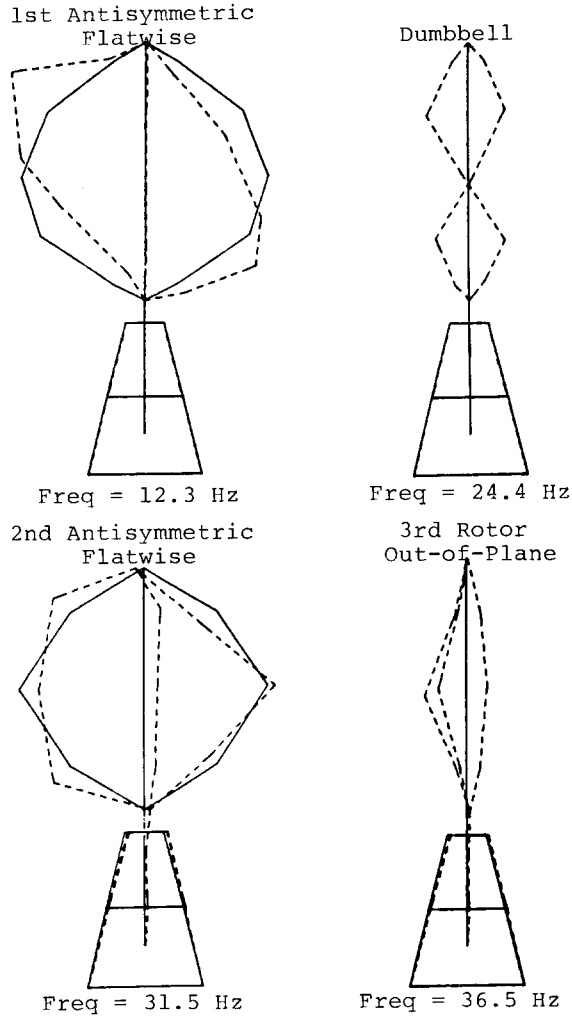

Fig. 11 Four Measured Mode Shapes for the Parked 2-m VAWT

Having obtained the modal characteristics of the parked turbine, the rotating modal test was conducted. Modal data was collected at six different rotational speeds in 100 rpm increments from 100 to 600 rpm. In this way, the changing frequencies could be tracked from their parked values up to the nominal operating speed of 600 rpm.

For the rotating test seven strain gages and two accelerometers were used to measure the response of the turbine. The two accelerometers were placed on tower in-the-plane and out-of-the-plane of the rotor. The steady-state centrifugal acceleration was sufficiently low on the tower so that accelerometers could be used conveniently. Two of the seven strain gages also were used on the tower with the other five on the blade roots. The strain gages, which have two active elements, were placed on the blades and tower so that they measured either purely in-plane or out-of-plane deformations. On the blades in-plane is generally referred to as flatwise (perpendicular to the blade chord), and out-of-plane as edgewise (in the direction of the chord).

Slip rings were used to transmit the transducer signals from the rotating turbine. However, before passing the signals through the slip rings, they were amplified by DC amplifiers mounted on the tower. In spite of the complications involved, transducers attached to the rotating structure were used so that the data taken would be relative to the rotating frame of the analytical predictions. Any measurements taken on fixed hardware would have to be transformed to the rotating frame for purposes of comparison. This process adds complexity to the data processing and cannot adequately determine blade behavior.

All testing in the rotating configuration was done in very low winds (less than 5 mph) to avoid aerodynamic excitation which could overwhelm the forces applied to excite modal response. In addition, the aerodynamic forces, which excite the turbine at integral multiples of the rotational frequency, might obscure any modal information at those frequencies. In the absence of wind, the motor-generator was used to propel the turbine and maintain its speed at a constant, preset value.

In selecting a device for exciting the rotating turbine, several concepts were considered. Any type of impact excitation is virtually eliminated because of the high blade tip speeds (over 190 ft/sec). Also, since this testing technique is to be applicable to turbines of all sizes, the device must be capable of exciting large turbines as well as the relatively small 2-m turbine used in this test.

The scheme finally chosen consists primarily of a pretensioned cable attached between one blade and the tower. The cable is suddenly released after the turbine is rotating at a preset speed. Figure 4 is a photograph of the turbine, showing the snap release device and the other instrumentation mentioned above. The snap release device consists of a force transducer which measures the tension in the cable, a burn wire, and an easily replaceable nylon cord. After preloading the cable, the turbine is rotated at the desired speed. A current is passed through the slipring to the burn wire which in turn cuts the nylon cord, releasing the tension in the cable. Figure 12 shows a detailed diagram of the snap-release device. The cable is restrained at both ends so that it becomes slack after release and does not fly out from the turbine.

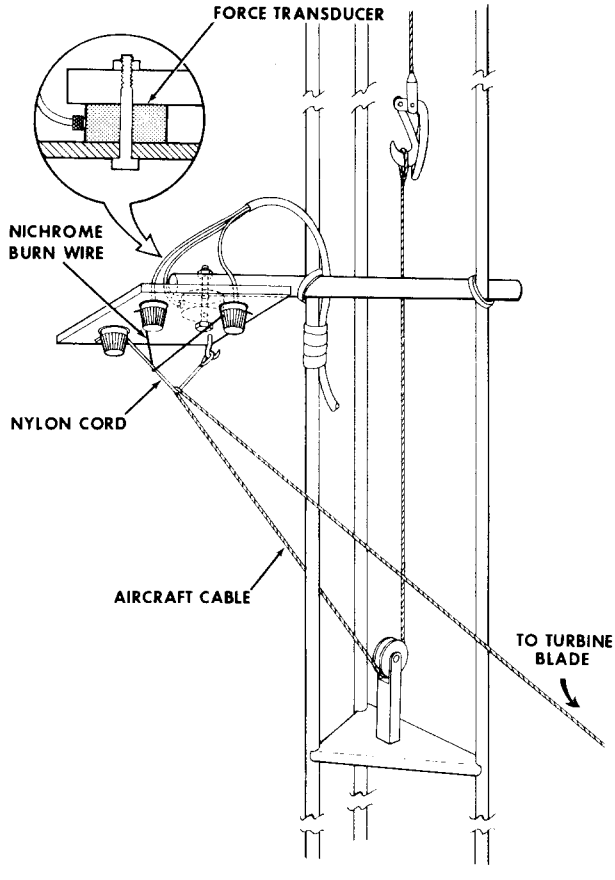

Fig. 12 The Snap-Release Device

It would appear that this snap-release device would only produce motion in the plane of the turbine, and this is the case for the parked turbine. However, when it is rotating, the in-plane and out-of-plane motions are coupled through Coriolis forces. Consequently, all modes of interest are excited by this mechanism.

One difficulty which is related to the FFT algorithm, arises in using this excitation device. The snap release basically applies a force which is a Heaviside function. As the Fourier transform for the Heaviside function does not exist, the FFT cannot be used on this force. However, if the Heaviside function is passed through a high-pass filter, it can be converted to a well behaved function that is easily transformable with the FFT. Figure 13 shows a trace of a typical force history after passing it through the high-pass filter. As shown, the force signal has dropped to essentially zero after about 0.4 sec., which is numerically compatible with the FFT. Also on this force trace, evidence exists (the three/rev response prior to release) that the turbine is being aerodynamically driven at some small level.

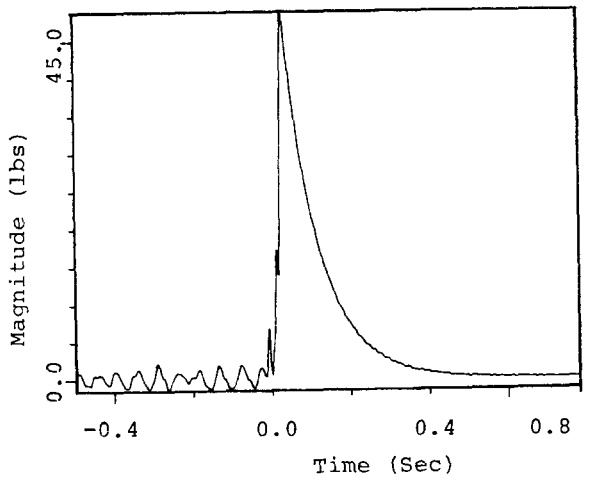

Fig. 13 A Typical Filtered Force History Produced by the Snap-Release Device

The high pass filter used in this test is the AC coupling circuit of the same set of amplifiers which amplify the signals before recording them on FM tape. Of course, the response signals must also pass through matched filters to avoid relative phase shifts between the response and the excitation. Figure 14 shows the magnitudes of the frequency response function for the low and high pass filters used here, with the three dB points at approximately 2.0 and 100.0 Hz.

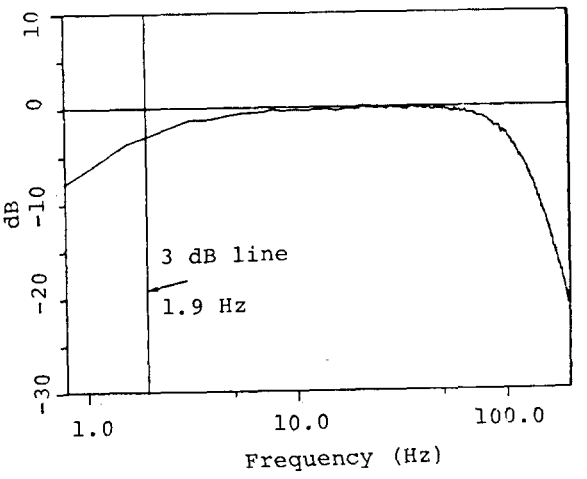

Fig. 14 The Magnitude of the Frequency Response Function for the Filter Used in the Rotating Modal Test

Figures 15 and 16 show typical frequency response functions from the rotating test at 600 rpm. These functions were obtained from data taken by in-plane and out-of-plane accelerometers located near the top of the tower. Taking into account the scale factors on the two plots, the magnitudes of the two response functions are approximately equal. This indicates that the Coriolis coupling has indeed produced out-of-plane response, even though the initial excitation was strictly in-plane.

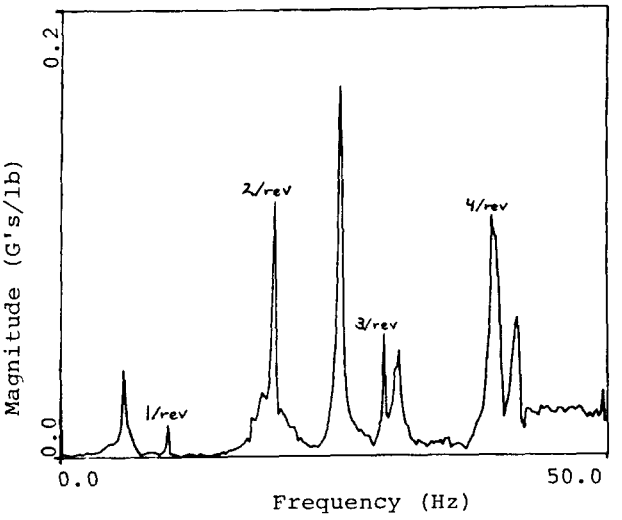

Fig. 15 Measured In-Plane Frequency Response Function for a Rotational Speed of 600 rpm

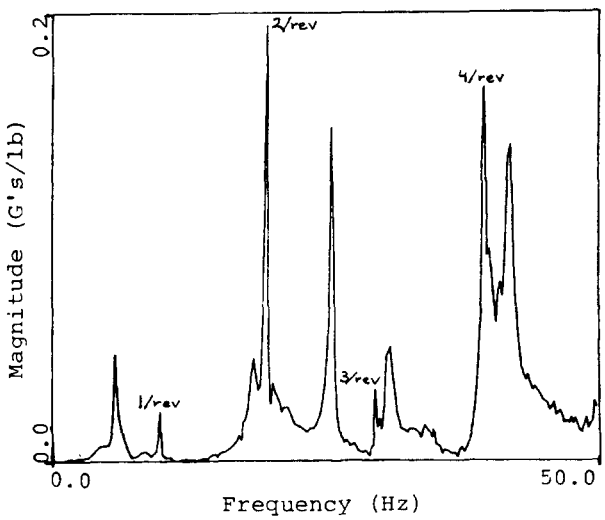

Fig. 16 Measured Out-of-Plane Frequency Response Function for a Rotational Speed of 600 rpm

Although the general data quality is represented by that in Figures 15 and 16, at higher rotational speeds the aerodynamic excitation of the turbine became more prevalent in spite of the low wind environment. This is indicated in the frequency response by high levels at integral multiples of the rotational frequency.

At each rotational speed, frequency response functions were computed from the data taken with the seven strain gages and the two accelerometers. Ignoring those peaks associated with the aerodynamic excitation, the frequencies of the remaining peaks on each of the response functions were extracted and tabulated. Small variations in the frequency of some of the modes did occur, and in those cases an average value was used. Since the mode shapes are complex, magnitude data were used rather than the imaginary component to obtain these modal frequencies.

In view of the small number of transducers on the turbine, a full description of the mode shape is impossible. However, eigenvectors can still be computed with nine components in each vector using the method outlined above. One typical eigenvector corresponding to the second rotor out-of-plane mode and a rotational speed of 300 rpm, is shown below. The magnitude and phase are separated by commas in the vector. The first two components are the accelerations with units of milli-g's, and the last seven are stresses with units of psi.

$$\begin{Bmatrix} \text{tower out-of-plane} \\ \text{tower in-plane} \\ \text{tower out-of-plane} \\ \text{tower in-plane} \\ \text{blade 1, lower edgewise} \\ \text{blade 1, upper edgewise} \\ \text{blade 2, lower edgewise} \\ \text{blade 2, upper edgewise} \\ \text{blade 2, lower flatwise} \end{Bmatrix} = \begin{Bmatrix} 1.00, & 90 \\ 1.28, & 166 \\ 7.57, & 279 \\ 4.25, & 178 \\ 1.06, & 249 \\ 0.83, & 275 \\ 1.12, & 256 \\ 0.80, & 255 \\ 0.00, & --- \end{Bmatrix}$$

This eigenvector has been normalized so that the first component has a unit magnitude and a phase of 90 degrees. Note the large phase variations which are normally not seen when non-rotating structures are analyzed for their complex modes. The out-of-plane acceleration has a phase of 76 degrees (nearly 90 degrees) greater than the in-plane acceleration. Likewise the out-of-plane tower strain gage is advanced by 101 degrees over the in-plane gage. The four edgewise strain gages are basically in phase with the out-of-plane deformation of the tower. These phase relationships are caused primarily by rotating coordinate system effects. Structural damping, errors from noise in the initial data and approximations in the extraction algorithms also contribute. However, from the phase components in the vector, it is clear that the in-plane and out-of-plane motion is approximately ninety degrees out of phase.

Comparison and Discussion of Results

The fan plot of Figure 7 which was generated for the 2-m turbine using the finite element predictive capability is reproduced in Figure 17. The experimental data are superimposed as shown. In general the agreement between the predicted and measured values is excellent. In fact, the average absolute deviation of the experimental points from the predicted is 0.52 Hz., or 2.2 percent. Although the deviation does not appear to be dependent on the rpm, the agreement is not as good at the higher frequencies. This degradation for the higher frequencies occurs in general when finite element methods are used and is primarily caused by an insufficient number of degrees of freedom in the model to accurately represent the associated mode shapes. The coarse representation of the base of the turbine may also be a contributor to this mild lack of agreement, especially since base motion was experimentally observed to be more prevalent in the higher modes.

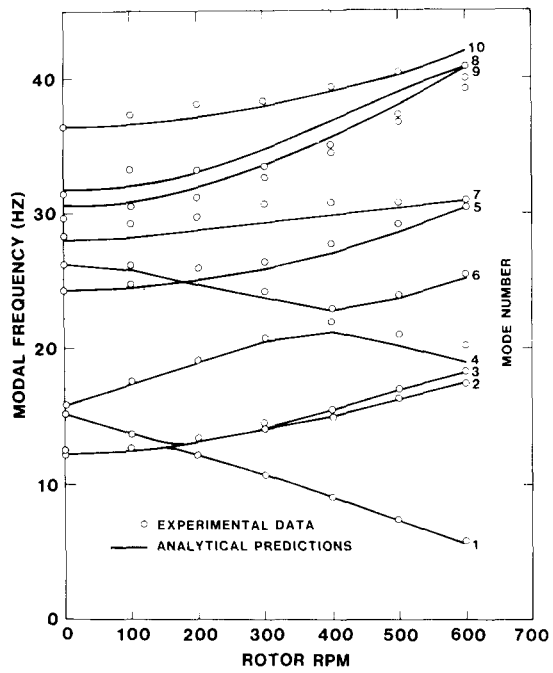

Fig. 17 A Comparison of Predicted and Measured Modal Frequencies for the 2-m VAWT as a function of rpm

Due to the small number of transducers on the turbine, the experimental mode shapes are coarse and quantitative comparisons to those predicted are difficult. However, as indicated in the previous section, the measured complex modes are definitely composed of in-plane and out-of-plane motion approximately ninety degrees out of phase, consistent with the predicted results.

Conclusions

In view of the excellent agreement between predicted and measured modal frequencies, the accuracy of the finite element technique for computing the modal characteristics of rotating VAWTs has been verified for lightly damped turbines. As shown, these predictions are of the same level of accuracy as is obtained in the finite element modal analysis of stationary structures. Additionally, a rotating modal testing technique for VAWTs has been demonstrated which is applicable to large as well as small turbines. Thus, if a predictive capability is unavailable, the rotating modal characteristics of established hardware can be measured by the technique described herein.

Acknowledgments

The authors wish to acknowledge W. N. Sullivan for providing the impetus to do the rotating modal test. C. M. Grassham made invaluable contributions in the design of the snap release device and in the planning and maintenance of the signal processing system. Others who made significant contributions in the testing and data reduction are P. H. Adams and his strain gage installation team, J. D. Burkhardt, B. K. Cloer, M. R. Weber, and L. H. Wilhelmi. Also, the work of J. R. Koteras in establishing special NASTRAN analysis procedures for the finite element predictive capability is gratefully acknowledged.

References

1. Hoa, S. V., "Vibration of a Rotating Beam with Tip Mass," Journal of Sound and Vibration, Vol. 67, No. 3, 1979, pp. 369-381.

2. Friedmann, P. P. and Straub, F., "Application of the Finite Element Method to Rotary Wing Aeroelasticity," Journal of the American Helicopter Society, Vol. 25, Jan. 1980, pp. 36-44.

3. Hodges, D. H. and Rutkowski, M. J., "Free-Vibration Analysis of Rotating Beams by a Variable-Order Finite-Element Method," AIAA Journal, Vol. 19, Nov. 1981, pp. 1459-1466.

4. Nigh, G. L. and Olson, M. D., "Finite Element Analysis of Rotating Disks," Journal of Sound and Vibration, Vol. 77, No. 1, 1981, pp. 61-78.

5. Patel, J. S. and Seltzer, S. M., "Complex Eigenvalue Solution to a Spinning Skylab Problem," NASA TMX-2378, Vol. II, Sept. 1971.

6. Klahs, J. W., Jr., and Ginsberg, J. H., "Resonant Excitation of a Spinning, Nutating Plate," Journal of Applied Mechanics, Vol. 46, March 1979, pp. 132-138.

7. Warmbrodt, W. and Friedmann, P., "Coupled Rotor/Tower Aeroelastic Analysis of Large Horizontal Axis Wind Turbines," AIAA Journal, Vol. 18, No. 9, 1980, pp. 1118-1124.

8. Vollan, A. J. and Zwaan, R. J., "Contribution of NLR to the First Phase of the National Research Program on Wind Energy, Part II: Elastomechanical and Aeroelastic Stability," National Aerospace Laboratory NLR, The Netherlands, NLR TR 77030 U Part II, March 1977.

9. Ottens, H. H. and Zwaan, R. J., "Description of a Method to Calculate the Aeroelastic Stability of a Vertical Axis Wind Turbine," National Aerospace Laboratory NLR, The Netherlands, NLR TR 78072 L, June 1978.

10. Ottens, H. H. and Zwaan, R. J., "Investigations on the Aeroelastic Stability of Large Wind Turbines," Proceedings of the Second International Symposium on Wind Energy Systems, Paper C3, Amsterdam, The Netherlands, Oct. 1978.

11. Hunter, W. F., "Integrating-Matrix Method for Determining the Natural Vibration Characteristics of Propeller Blades," NASA TN D-6064, Dec. 1970.

12. Carpenter, J. E. and Sullivan, E. M., "Structural and Vibrational Characteristics of WADC S-5 Model Propeller Blades," WADC Tech. Rep. 56-298, DDC AD 130 787, U. S. Air Force, June 1957.

13. Popelka, D., "Aeroelastic Stability of a Darrieus Wind Turbine," Sandia National Laboratories, SAND82-0672, March 1982.

14. Dettman, J. W., Mathematical Methods in Physics and Engineering, Second Edition, McGraw-Hill Book Co., New York 1969, p. 43.

15. MSC/NASTRAN User's Manual, Vols. I and II, The MacNeal-Schwendler Corporation, Los Angeles, 1981.

16. Klosterman, A. L. and Zimmerman, R., "Modal Survey Activity Via Frequency Response Functions," SAE Paper No. 751068, National Aerospace Engineering and Manufacturing Meeting, Culver City, Nov. 1975.

17. Modal-Plus Reference Manual, Version 6, The SDRC Corporation, Milford, Ohio, Aug. 1981.